Optical Materials 138 (2023) 113619

Contents lists available at ScienceDirect

Optical Materials

journal homepage: www.elsevier.com/locate/optmat

Research Article

Influence of chirality on the aggregation of a new A-π-D-π-A small molecule with a benzodithiophene core: Spectroscopic and morphological investigations

Francesca Parenti [a,*], Raffaella Capelli [b,c], Adele Mucci [a], Cecilia Mortalò [d], Guido Paolicelli [e], Laura Pigani [a], Davide Vanossi [a], Monica Caselli [a]

[a] Department of Chemical and Geological Sciences, University of Modena and Reggio Emilia, Via Campi 103, 41125, Modena, Italy
[b] Department of Engineering "Enzo Ferrari" (DIEF), University of Modena and Reggio Emilia, Via P.Vivarelli 10, 41125, Modena, Italy
[c] Department of Physics, University of Johannesburg, PO Box 524, Auckland Park, 2006, South Africa
[d] Institute of Condensed Matter Chemistry and Energy Technologies (ICMATE), National Research Council of Italy, C.so Stati Uniti 4, IT-35127, Padova, Italy
[e] CNR Institute Nanoscience (NANO), Via Campi 213, 41125, Modena, Italy

A B S T R A C T

In this paper, the synthesis and characterization of a new alkoxy benzodithiophene-based small molecule bearing two stereocenters and two end-capping acetyl groups (**BDTCOR**) are reported. The molecule has been obtained in both enantiopure form (S, S) and stereoisomeric mixture. The spectroscopic properties of **BDTCOR** in solution were compared to computational data revealing that the molecule is a candidate for optoelectronic applications thanks to a broad UV–Vis absorption spectrum and suitable fluorescence properties. The molecule was deposited as a thin film by physical vapor deposition on SiO_2 and PMMA substrates revealing a quite different behavior of the enantiopure form vs. the stereoisomeric mixture. In particular, significant differences were found in film morphology suggesting that, contrary to what observed for the stereoisomeric mixture, enantiopure **BDTCOR** tends to generate supramolecular well-ordered structures. Moreover, while electronic circular dichroism spectra of enantiopure **BDTCOR** casted films do not show significant signals, vapor-deposited films show intense Cotton effect, suggesting a synergic role of chirality and of the deposition technique on the molecular order.

1. Introduction

Small molecules possessing a wide π-conjugated system are an interesting class of organic semiconductors finding application in numberless optoelectronic devices [1,2]. They boast several properties such as high charge mobility and polarizability, good solubility and filmability; moreover, they show low-energy broad absorption bands and, with respect to their corresponding polymers, they display a well-defined structure. In addition, they are prone to organize themselves in ordered supramolecular structures [3]; this is often a key feature that influences the electro-optical properties (such as light absorption and emission, charge transport and exciton transfer) and, ultimately, the efficiency of optoelectronic devices (i.e. small-molecules based solar cells [4,5], dye sensitized solar cells [6], organic field effect transistors [7]).

Within the plethora of different molecular structures reported in the literature, benzo[1,2-*b*:4,5-*b'*]dithiophene (**BDT**)-based materials are widely studied [8–10] thanks to their relative ease of synthesis, stability and structure rigidity. Furthermore, the two benzenic para positions are susceptible of further functionalization, for instance with branched alkoxy chains or conjugated groups, in order to ensure good solubility and to tune the molecular orbital energy levels of the resulting molecules [11]. Moreover, thanks to the presence of the π-conjugated core, **BDT**-based small molecules can effectively promote the intermolecular charge hopping process. In particular, as a function of the chemical tailoring, they have been demonstrated to work both as p-type and n-type semiconductors [12,13]. Lastly, **BDT** derivatives form well-ordered films by physical vapor deposition technique [14]. This interesting feature opens new perspectives in their use in devices where the film order plays a crucial role, such as in organic photovoltaics [15–17]and optoelectronic devices, such as organic thin film transistors [18,19]and light emitting diodes.

In this paper we present the synthesis, the spectroscopic and electrochemical properties together with the morphological analysis of a BDT-based small molecule possessing two stereocenters (Scheme 1 **BDTCOR**). This displays a typical A-π-D-π-A architecture with a central alkoxy benzodithiophene (**BDTA**) electron donor core and two terminal keto electron acceptors units, bound by two π bridges. While the

* Corresponding author.
E-mail address: francesca.parenti@unimore.it (F. Parenti).

https://doi.org/10.1016/j.optmat.2023.113619
Received 22 December 2022; Accepted 20 February 2023
Available online 7 March 2023

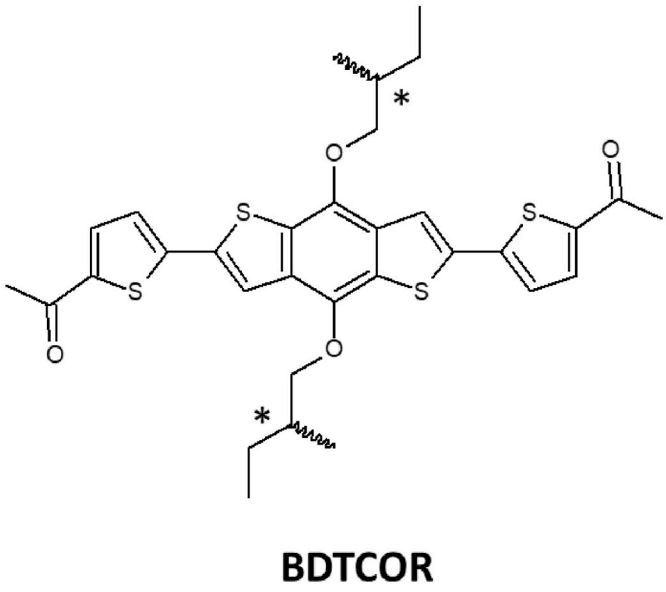

Scheme 1. The investigated small molecule, **BDTCOR**: asterisks denote the stereocenters.

alternance of donor and acceptor units should contribute to lower the band gap and to widen [20,21] the absorption spectra, the chirality of the alkoxy substituent could play a role in the supramolecular organization of the molecule. To this purpose, we have synthesized **BDTCOR** in the enantiopure, optically active, form (S,S) (denoted as (+)-**BDTCOR** in Scheme 2) and in the stereoisomeric, optically inactive, mixture (denoted as (±)-**BDTCOR** in Scheme 2) and investigated the role played by the chirality in the optical properties and in the morphology of the films obtained by thermal evaporation. From the electronic circular dichroism (ECD) spectra recorded both in solution and in solid state (film by casting and physical vapor deposition) it was possible to observe a quite different behavior of the enantiopure vs the stereoisomeric mixture, clearly showing that chirality plays a key role at the supramolecular level, especially when physical vapor deposition is used as the deposition technique.

Despite being a relatively simple small molecule, **BDTCOR** exhibits interesting properties such as a broad absorption band in the visible region, which is a fundamental requisite for an efficient harvesting of solar radiation, a good thermal stability that permits the film formation by thermal evaporation technique, and, in its optically active form, a proneness to organize itself in chiral aggregates. We are confident that these results may spur further studies in the use of similar **BDT** derivatives in optoelectronics or photovoltaics. Indeed, as already observed with similar molecules [22,23], enantiopure (+)-**BDTCOR** could behave as a new chiral dopant in polymeric active materials for circular polarized light-emitting devices [24–27], the circularly polarized light emission being of interest in several areas such as high efficiency displays [28], optical quantum computing [29] and biosensing [30].

2. Materials and methods

2.1. Measurements and instruments

Medium Pressure Liquid Chromatography (MPLC) was performed with a Grace Reveleris Flash Chromatography system with evaporative light scattering (Alltech 3300 ELSD) and UV detection. ^{1}H and ^{13}C NMR spectra were recorded with Bruker Avance 400 and Avance III HD 600 spectrometers, operating at 400.13 and 600.13 MHz for proton and at 100.61 and 150.90 MHz for carbon, respectively. Assignments were made also applying standard HSQC and HMBC pulse sequences.

UV–vis spectra were collected using a Varian Cary 100 Scan UV–vis spectrophotometer. Fluorescence spectra were measured with a Horiba Jobin Yvon Fluoromax-3 spectrofluorometer; the spectra were corrected for the instrumental spectral sensitivity. Fluorescence quantum yields (Φ_F) were determined at room temperature using fluorescein in NaOH 0.1 M as the standard (Φ_F = 0.925 [31]). The correction for the refractive index of the solvents was introduced. Fluorescence lifetimes (τ_F) were measured with a Horiba FluoroMax4 time correlated single-photon counting equipment using, as the excitation source, a nano-LED that emits at 450 nm. Films deposited by physical evaporation on 12.5 × 45 mm quartz substrates were used for the spectroscopic measurements. Fluorescence measurements of the films were performed with a front-face illumination using a solid sample cell holder with variable angle. The incidence angle of excitation radiation on the sample was 60°. All the calculations on BDTCOR molecule were carried out using Orca 5 (release 5.02) Quantum Chemistry package [32,33]. Assuming a standard structure as a starting point, the ground state (S_0) geometry of BDTCOR was fully optimized at DFT B3LYP/def2-SVP level. We checked for the positive semidefinite character of the nuclear hessian in order to ensure that the located stationary point was a true local minimum. Starting from this gas-phase optimized structure, we employed the Adiabatic Linear-Response TDDFT (A-LR-TDDFT)

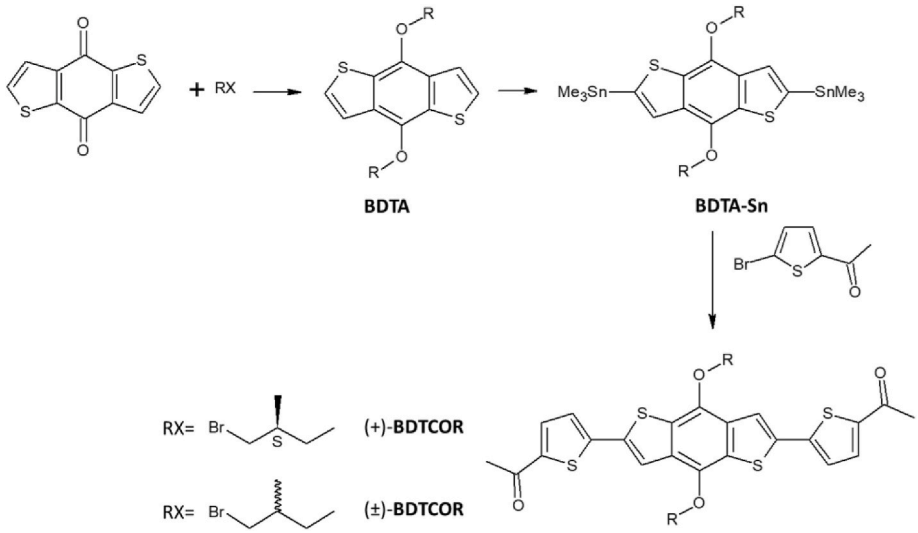

Scheme 2. The synthetic pathway followed for the synthesis of (+)-**BDTCOR**] and (±)-**BDTCOR**.

methodology to calculate the gas-phase one-photon absorption (OPA) spectrum. This task was accomplished using both B3LYP/def2-SVP and the more refined B3LYP/def2-TZVP level of the theory. Aiming at investigating also the emission property of BDTCOR, from the first excited singlet state S_1, a rather similar computational recipe was considered. First, we optimized the gas-phase S_1 structure at A-LR-TDDFT B3LYP/def2-SVP level; then, the one-photon emission (OPE) spectrum was also obtained using the A-LR-TDDFT B3LYP/def2-TZVP description. For the sake of comparison with spectroscopic experimental data, we incorporated in the aforementioned computational strategy the solvent effects in the framework of Polarizable Continuum Model (PCM) [34] at the linear-response CPCM level available in Orca 5 [35]. Electronic circular dichroism (ECD) spectra were recorded with a JASCO J-710 spectropolarimeter with 1 cm path length. Cyclic voltammetry (CV) was conducted in an acetonitrile solution containing 0.1 M tetraethylammonium hexafluorophosphate ($TEAPF_6$) (puriss., Fluka) as the supporting electrolyte. The measurements were carried out in a three electrodes cell in a dry argon atmosphere using an Autolab PGSTAT 12 galvanostat/potentiostat (Eco Chemie). A 3-mm-diameter Pt disk (Metrohm) was used as the working electrode. A glassy carbon and an Ag/AgCl electrode were the auxiliary and the reference electrodes, respectively. Topographical analysis was carried out by using a commercially Atomic Force Microscope (AFM) from NT-MDT, mod. NTEGRA AURA. All the measurements were performed in air, under ambient conditions (T ≈ 25 °C, RH ≈ 55%) using commercially available rectangular shaped silicon cantilevers with nominal elastic constants between 0.3 and 0.8 N m^{-1} (MikroMasch HQ: CSC37/NoAl). Topography images were recorded in semi-contact mode (tapping mode) @ 1 Hz scan rate. Images size typical 512 × 512 points. Tip apexes were estimated regularly by performing a deconvolution of the topography obtained on an AFM calibration sample (PA01/NM). Typical apex radius is about 10–15 nm. For the preparation of the films two different techniques were considered: a few hundred nanometers thick PMMA film was spin-coated on top of pre-cleaned glass substrates, while a commercial film of SiO_2 thermally deposited on a Si wafer has been used. Before the deposition of the compounds of interest, substrates were deeply cleaned by subsequent ultrasonic treatments in organic solvents. Contact angle has been measured on cleaned substrates obtaining a value of about 70° for both SiO_2 and PMMA, which indicates a similar average surface polarity for both surfaces. Thin films of different thicknesses were then grown by high vacuum sublimation keeping the substrate at room temperature.

2.2. Synthesis

2-acetyl-5-bromothiophene (99%) was purchased from Sigma Aldrich, benzo[1,2-b:4,5-b']dithiophene-4,8-dione was obtained as already reported [36]. Dichloromethane and toluene were dried by standing over 4 Å molecular sieves for at least 24 h, THF was distilled from Na-benzophenone just before use.

(S,S)-(+)-4,8-bis(2-methyl-1-butyloxy)benzo[1,2-b:4,5-b']dithiophene [(+)-BDTA]. In a Schlenk tube under argon atmosphere, 0.50 g (2.3 mmol) of benzo[1,2-*b*:4,5-*b*']dithiophene-4,8-dione, tetrabutylammonium bromide (0.22 g, 0.68 mmol) and a first portion of zinc powder (0.38 g, 5.8 mmol) were suspended in 14 mL of water. Under stirring, 1.36 g of NaOH (34 mmol) were added and the mixture was refluxed for 1 h (the solution turns to red). After this (*S*)-(+)-1-bromo-2-methylbutane was added (1.03 g, 6.8 mmol) and the mixture was refluxed for another 3 h (the solution turns to dark red then to yellow). A second portion of zinc powder was then added (0.15 g, 2.3 mmol) (the solution turns to green) and the mixture was refluxed overnight. The resulting yellow solution was poured into iced water and extracted with diethylether (3 × 10 mL) then the combined organic layers were dried with anhydrous $MgSO_4$ and evaporated under reduced pressure. The crude was purified by MPLC chromatography (40 g silica gel column, hexane: dichloromethane 3:1) yielding a light-yellow oil (0.24 g, 29%). $[\alpha]_D^{20} = +5.65$ (c = 0.0099, dichloromethane).

^{1}H NMR (400 MHz, Acetone) δ 7.63 (d, *J* = 5.6 Hz, 1H), 7.55 (d, *J* = 5.6 Hz, 1H), 4.18 (dd, *J* = 9.0, 5.7 Hz, 1H), 4.11 (dd, *J* = 9.0, 6.2 Hz, 1H), 1.95 (oct, average *J* = 6.2 Hz, 1H), 1.74 (ddq, *J* = 13.4, 5.6, 7.5 Hz, 1H), 1.39 (dqn, 13.4, 7.5 Hz, 2H), 1.16 (d, *J* = 6.8 Hz, 3H), 1.02 (t, *J* = 7.5 Hz, 3H).

(±)-4,8-bis(2-methyl-1-butyloxy)benzo[1,2-b:4,5-b']dithiophene [(±)-BDTA]. It was synthesized in the same way as **(+)-BDTA** starting from 0.66 g (3.0 mmol) of benzo[1,2-*b*:4,5-*b*']dithiophene-4,8-dione and 1.37 g (9.1 mmol) of racemic (±)-1-bromo-2-methylbutane. A light-yellow oil was obtained 0.28 g (25% yield).

^{1}H NMR (400 MHz, Acetone) δ 7.63 (d, *J* = 5.6 Hz, 1H), 7.55 (d, *J* = 5.6 Hz, 1H), 4.18 (dd, *J* = 9.0, 5.7 Hz, 1H), 4.11 (dd, *J* = 9.0, 6.2 Hz, 1H), 1.95 (oct, average *J* = 6.2 Hz, 1H), 1.74 (ddq, *J* = 13.4, 5.6, 7.5 Hz, 1H), 1.39 (dqn, 13.4, 7.5 Hz, 2H), 1.16 (d, *J* = 6.8 Hz, 3H), 1.01 (t, *J* = 7.5 Hz, 3H).

(S,S)-2,6-Bis(trimethyltin)-4,8-bis(2-methyl-1-butyloxy)benzo [1,2-b:4,5-b']dithiophene [(+)-BDTA-Sn]. In a three neck round bottom flask, equipped with argon inlet, perforable septum and thermometer, a solution of **(+)-BDTA** (0.24 g, 0.66 mmol) in 6 mL of anhydrous THF was cooled to −78 °C. A butyllithium solution (1.6 M in hexane, 0.90 mL, 1.4 mmol) was added dropwise with stirring and the mixture was kept at −78 °C for 1/2 h and at rt for 2 h. The solution was re-cooled to −78 °C then a trimethyl tin chloride solution (1 M in hexane, 1.56 mL) was added in one portion. The mixture was stirred at rt overnight then it was poured into iced water and extracted with diethyl ether (3 × 15 mL). The combined organic phases were washed with water (2 × 20 mL), dried with anhydrous $MgSO_4$ and evaporated to dryness in vacuum. The crude was purified by washing with 5 mL of methanol with the help of an ultrasonic bath (5 min): after filtration, a white solid was obtained (0.26 g, 38%) which was immediately used without further purification.

^{1}H NMR (400 MHz, $CDCl_3$) δ 7.52 (s, $^2J_{H,\,Sn}$ = 29.4 Hz, 2H), 4.17 (dd, *J* = 9.1, 5.8 Hz, 2H), 4.08 (dd, *J* = 9.1, 6.5 Hz, 2H), 1.99 (oct mean *J* = 6.5 Hz, 2H), 1.75 (ddq, *J* = 13.6, 5.5, 7.5 Hz, 2H), 1.38 (dqn, *J* = 13.6, 7.5 Hz, 2H), 1.16 (d, *J* = 6.8 Hz, 6H), 1.02 (t, *J* = 7.5 Hz, 6H), 0.45 (s, $^2J_{H,117Sn/H,119Sn}$ = 55.3, 57.7 Hz, 18H).

(±)-2,6-Bis(trimethyltin)-4,8-bis(2-methyl-1-butyloxy)benzo[1,2-b:4,5-b']dithiophene [(±)-BDTA-Sn]. It was synthesized in the same way as **(+)-BDTA-Sn** starting from 0.32 g (0.88 mmol) of **(±)-BDTA**, 1.2 mL of butyllithium solution and 2.10 mL of trimethyl tin chloride solution. A white solid was obtained (0.26 g, 21%).

^{1}H NMR (400 MHz, $CDCl_3$) δ 7.52 (s, $^2J_{H,\,Sn}$ = 29.4 Hz, 2H), 4.17 (dd, *J* = 9.1, 5.8 Hz, 2H), 4.08 (dd, *J* = 9.1, 6.5 Hz, 2H), 1.99 (oct, mean *J* = 6.5 Hz, 2H), 1.75 (ddq, *J* = 13.6, 5.5, 7.5 Hz, 2H), 1.38 (dqn, *J* = 13.6, 7.5 Hz, 2H), 1.16 (d, *J* = 6.8 Hz, 6H), 1.02 (t, *J* = 7.5 Hz, 6H), 0.45 (s, $^2J_{H,117Sn/H,119Sn}$ = 55.3, 57.7 Hz, 18H).

(+)-BDTCOR. In a Schlenk tube, under inert atmosphere, a dried toluene solution (15 mL) of **(+)-BDTA-Sn** (0.22 g, 0.32 mmol) and 2-acetyl-5-bromothiophene (0.14 g, 0.67 mmol) was accurately degassed by argon bubbling (15 min). Then 0.037 g (0.032 mmol) of tetrakis (triphenylphosphine)-palladium(0) were added and the mixture heated (100 °C) under stirring for 48 h. After cooling to rt, the mixture was poured in water, extracted with 20 mL of dichloromethane and the organic layer was washed with water (2 × 10 mL), dried over $NaSO_4$ and evaporated to dryness. An orange solid was obtained which was carefully washed with MeOH (2 × 5 mL) (0.16 g, 82%). $[\alpha]_{D20} = +15.5$ (c = 0.0129, dichloromethane).

^{1}H NMR (400 MHz, DMSO) δ 7.96 (d, *J* = 4.0 Hz, 1H, H4′), 7.88 (s, 1H, H3)), 7.69 (d, *J* = 4.0 Hz, 1H, H3′), 4.19 (dd, *J* = 9.1, 5.8 Hz, 1H, OC*H*H), 4.12 (dd, *J* = 9.1, 6.3 Hz, 1H, OCH*H*), 2.56 (s, 3H, CH_3CO), 1.93 (oct, average *J* = 6.6 Hz, 1H, CH), 1.68 (ddq, *J* = 13.6, 5.6, 7.5 Hz, 1H, C*H*HCH_3), 1.35 (dqn, *J* = 13.6, 7.5 Hz, 1H, C*H*HCH_3), 1.12 (d, *J* = 6.8 Hz, 3H, C*H*$_3$CH), 0.99 (t, *J* = 7.5 Hz, 3H, C*H*$_3$CH$_2$). ^{13}C NMR (400 MHz, DMSO) δ 190.6 (C═O), 144.0 (C4), 143.7 (C5′), 143.4 (C2′), 135.6 (C2), 135.0 (C4′), 131.5 (C3a), 129.3 (C4a), 127.3 (C3'), 118.6 (C3), 78.6 (OCH_2), 35.3 (CH), 26.4 (CH_3CO), 25.4 (CH_2CH_3), 16.3 (CH_3CH), 11.3

(CH_3CH_2).

(±)-BDTCOR. It was synthesized in the same way as **(+)-BDTCOR** starting from 0.19 g (0.28 mmol) of **(±)-BDTA-Sn**, 0.14 g (0.59 mmol) of 2-acetyl-5-bromothiophene and 0.032 g (0.028 mmol) of tetrakis (triphenylphosphine)-palladium(0). An orange solid was obtained which was carefully washed with MeOH (2 × 5 mL) (0.15 g, 88%).

^{1}H NMR (400 MHz, DMSO) δ 7.96 (d, J = 4.0 Hz, 1H, H4′), 7.88 (s, 1H, H3)), 7.69 (d, J = 4.0 Hz, 1H, H3′), 4.19 (dd, J = 9.1, 5.8 Hz, 1H, OC*H*H), 4.12 (dd, J = 9.1, 6.3 Hz, 1H, OCH*H*), 2.56 (s, 3H, CH_3CO), 1.93 (oct, average J = 6.6 Hz, 1H, CH), 1.68 (ddq, J = 13.6, 5.6, 7.5 Hz, 1H, C*H*HCH$_3$), 1.35 (dqn, J = 13.6, 7.5 Hz, 1H, C*H*HCH$_3$), 1.12 (d, J = 6.8 Hz, 3H, C*H*$_3$CH), 0.99 (t, J = 7.5 Hz, 3H, C*H*$_3$CH$_2$). ^{13}C NMR (400 MHz, DMSO) δ 190.6 (C═O), 144.0 (C4), 143.7 (C5′), 143.4 (C2′), 135.6 (C2), 135.0 (C4′), 131.5 (C3a), 129.3 (C4a), 127.3 (C3'), 118.6 (C3), 78.6 (OCH_2), 35.3 (CH), 26.4 (CH_3CO), 25.4 (CH_2CH_3), 16.3 (CH_3CH), 11.3 (CH_3CH_2).

3. Results and discussion

3.1. Synthesis

The synthetic pathway for the obtainment of (+)-**BDTCOR** and (±)-**BDTCOR** is depicted in Scheme 2. We started from commercially available benzo[1,2-*b*:4,5-*b*']dithiophene-4,8-dione, which was reduced with zinc dust in water and in the presence of tetrabutylammonium bromide as phase transfer catalyst. Subsequent addition of the enantiopure or racemic halogenoalkane (RX), afforded the corresponding alkoxy substituted benzodithiophene **BDTA** in 29 and 25% yield, respectively. Enantiopure **BDTA** and its stereoisomer mixture were then treated in THF at −78 °C with butyllithium and the alpha deprotonated thiophenes obtained were in turn reacted with trimethyltin chloride affording the corresponding stannylated derivative **BDTA-Sn**. Each of the latter derivatives was coupled, under Stille conditions, with commercially available 2-bromoacetylthiophene to give (+)-**BDTCOR** and (±)-**BDTCOR** as orange solids in 82 and 88% yield, respectively. **BDTCORs** are soluble in common organic solvents such as cyclohexane, tetrahydrofuran, ethyl acetate, acetonitrile, acetone, dichloromethane and dimethylsulfoxide, were they form intensely colored solutions.

3.2. Optical and photophysical properties

The spectroscopic and photophysical properties of **(+)-BDTCOR** and **(±)-BDTCOR** are, as expected, identical in solution. The absorption and emission maxima, the relative absorption molar coefficients and the Stokes shift are reported in Table 1. The absorption spectra in organic solvents (Fig. 1) are characterized by two intense structured bands above 300 nm, one between about 425 and 455 nm, the other between about 370 and 395 nm, which are essentially independent of the solvent polarity. These results are expected on the basis of the calculated electric dipole moments, which result close to zero (see below).

Table 1
Experimental absorption and fluorescence maxima, molar absorption coefficients, Stokes shift of **BDTCOR**.

Solvent	λ_{abs}^{max} (nm)	λ_{fl}^{max} (nm)	Stokes shift (cm^{-1})
cyclohexane	377,388,429,453	520	2845
ethyl acetate	377,388,428,449	553	4188
tetrahydrofuran	379,390,431,452 ε^{452} = 24700 $M^{-1}cm^{-1}$	560	4266
dichloromethane	~388,437,456	597	5180
acetonitrile	~382,430,448	612	5981
dimethyl sulfoxide	~388,437,457	612	5542
Film (±)-**BDTCOR**	306,388(s),406,454,486	573	
(+)-**BDTCOR**	307,388(s),411, 460,497	558	

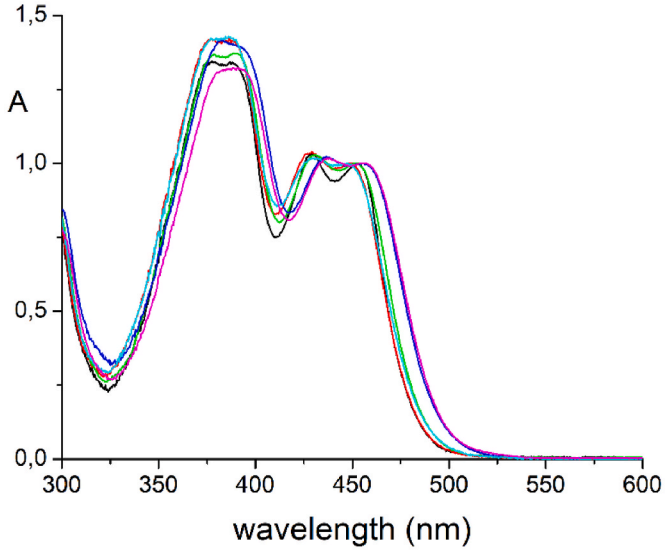

Fig. 1. Normalized absorption spectra of **BDTCOR** in cyclohexane (black), ethyl acetate (red), tetrahydrofuran (green), dichloromethane (blue), acetonitrile (cyan), dimethyl sulfoxide (magenta).

The gas-phase DFT equilibrium geometries of **BDTCOR** (Fig. S1) show that the molecule is characterized by an essentially coplanar structure, except for the alkoxy substituents, which are orthogonal to the plane of the **BDTA** core. The thienyl groups form an angle of 11° with the **BDTA** core in the S_0 state and of 2.5° in the S_1 state, hence characterized by an increased planar structure. The calculated ground-state electric dipole moment is very low, reflecting the symmetry of the compound, and does not significantly change in the first excited state S_1 (Table S1).

The calculated spectrum in the gas phase (Table 2) evidences two intense electronic transitions close to the experimental wavelength ranges, as well: the first one, which is dominated by an [H,L] character, is located at about 490 nm, while the second, mainly attributed to a [(H-1),L] excitation, is found approximately at 410 nm.

The calculated maxima are in rather good agreement with the positions of the two experimental electronic absorption bands (Table 1), which show also a blurred vibrational structure.

The introduction of the solvent effects in the calculations (Table S2) causes only a small reduction of the transition energy. The molecular orbitals involved in both electronic transitions are widely delocalized over the whole structure (Fig. S2). Therefore, both the [H,L] and the [(H-1),L] electronic transitions do not possess a relevant charge transfer character: Fig. S2 shows a low charge transfer character from the **BDTA** core to the acetyl groups.

The fluorescence emission spectra of **BDTCOR** (Fig. 2) are independent of the excitation wavelength in any solvent (Fig. S3); the excitation fluorescence spectra, almost independent of emission wavelength, reproduce fairly well the absorption spectra (Fig. S4). Such findings indicate that only one species, capable of absorbing and fluorescing, is present in solution.

The calculated emission spectra, both in the gas phase and in solution, are in a rather good agreement with the experimental ones (Tables 3 and 4).

It is apparent from Fig. 2 that, contrary to what observed for the absorption spectra (Fig. 1), the fluorescence ones show a positive solvatochromic shift: from cyclohexane to acetonitrile/dimethyl sulfoxide they are red-shifted of about 85 nm and a parallel increase of the Stokes shift can be detected. Such a behavior, often observed in V-shaped molecules [37], can be interpreted according to the excited-state symmetry breaking model, originally proposed for quadrupolar molecules [38].

BDTCOR is characterized by a quite high fluorescence quantum yield

Table 2
A-LR-TDDFT OPA gas-phase properties for singlet excited states of **BDTCOR**: state and composition, transition energy (ΔE), oscillator strength (f). The OPA features only for electronic transitions characterized by $f \geq 0.1$ are reported, considering just the first six excited states in the calculations. The absorption was calculated starting from the optimized (B3LYP/def2-SVP) S_0 ground state structure.

Molecule	B3LYP/def2-SVP			B3LYP/def2-TZVP		
	(state): composition	ΔE/eV (nm)	f	(state): composition	ΔE/eV (nm)	f
BDTCOR	(S_1): 0.97[H,L] (S_3): 0.95[H-1,L]	2.61 (474.4) 3.11 (399.3)	0.763 0.818	(S_1): 0.97[H,L] (S_3): 0.95[H-1,L]	2.54 (489.0) 3.02 (410.7)	0.752 0.771

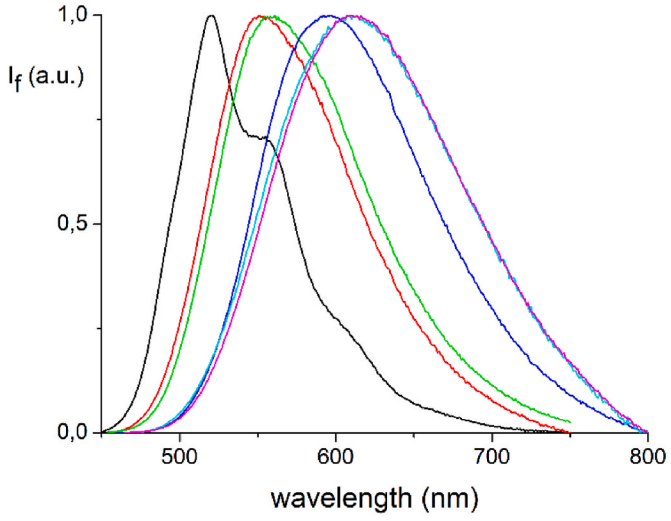

Fig. 2. Corrected normalized fluorescence spectra of **BDTCOR** in cyclohexane (black), ethyl acetate (red), tetrahydrofuran (green), dichloromethane (blue), acetonitrile (cyan), dimethyl sulfoxide (magenta).

Table 3
A-LR-TDDFT OPE gas-phase properties of **BDTCOR**: transition type, transition energy (ΔE), oscillator strength (f). The emission was calculated starting from the S_1 optimized (A-LR-TDDFT B3LYP/def2-SVP) structure.

Molecule	B3LYP/def2-SVP			B3LYP/def2-TZVP		
	Transition	ΔE/eV (nm)	f	Transition	ΔE/eV (nm)	f
BDTCOR	$S_1(\pi_H\pi_L^*)\rightarrow S_0$	2.23 (555.4)	0.603	$S_1(\pi_H\pi_L^*)\rightarrow S_0$	2.17 (572.7)	0.591

Table 4
A-LR-TDDFT OPE properties of **BDTCOR** calculated considering solvent-effects at LR-CPCM level: transition, transition energy (ΔE) and oscillator strength (f). The OPE features for the $S_1 \rightarrow S_0$ electronic transitions are only reported. The emission was calculated from the optimized (A-LR-TDDFT B3LYP/def2-SVP) S_1 excited state structure in presence of the solvent.

Solvent	B3LYP/def2-SVP			B3LYP/def2-TZVP		
	Transition	ΔE/eV (nm)	f	Transition	ΔE/eV (nm)	f
cyclohexane	$S_1(\pi_H\pi_L^*)\rightarrow S_0$	2.34 (530.1)	1.19	$S_1(\pi_H\pi_L^*)\rightarrow S_0$	2.26 (548.6)	1.18
acetonitrile	$S_1(\pi_H\pi_L^*)\rightarrow S_0$	2.17 (571.4)	1.59	$S_1(\pi_H\pi_L^*)\rightarrow S_0$	2.21 (561.0)	1.16
dimethyl sulfoxide	$S_1(\pi_H\pi_L^*)\rightarrow S_0$	2.17 (571.4)	1.60	$S_1(\pi_H\pi_L^*)\rightarrow S_0$	2.20 (563.6)	1.23

(0.15–0.20), substantially independent of the solvent, with the exception of dichloromethane, where a little higher fluorescence quantum yield is observed (Table 5). Fluorescence lifetimes show a biexponential decay, characterized by a shorter component (0.8–1 ns) and a longer one

Table 5
Photophysical properties of **BDTCOR** in solution.

solvent	Φ_F	τ_{F1} (ns)	τ_{F2} (ns)
cyclohexane	0.15	0.8	
ethyl acetate	0.15	1.0	2.3
tetrahydrofuran	0.17	0.2	2.3
dichloromethane	0.28	1.1	2.7
acetonitrile	0.16	1.3	2.5
dimethyl sulfoxide	0.20		2.6

(2.3–2.7 ns), whose relative abundances, deduced by the preexponential factors, are dependent on the solvent.

In order to investigate the relationship between the chemical structure and the spectroscopic properties of **BDTCOR**, an analysis of the role played by the building blocks and the substituents in apolar solvents has been performed. By comparison of the absorption spectrum of **BDTCOR** with that of **BDT**, a marked bathochromic shift of the low-energy band can be observed, from 336 nm for **BDT** [39] to 455 nm for **BDTCOR**. The introduction of the alkoxy groups on the benzene ring of **BDT** induces a slight bathochromic shift (experimental about 15 nm [40] and calculated about 11 nm, Table S3) of the low-energy absorption band and molecular orbital pictures (Fig. S2) show that a partial conjugation of the alkoxy groups with the **BDT** core takes place. The further substitution of **BDTA** in position 2,6- with thienyl groups induces an important bathochromic shift (about 60 nm) that leads the absorption maximum to 413 nm [40]. The acetyl group in **BDTCOR** has an important role, causing a further bathochromic shift of the absorption maximum to about 455 nm.

The absorption properties of **BDTCOR** can be mainly attributed to the increase of the conjugation pathway related to the presence of thienoacetyl groups (Fig. S2), as already observed in similar systems that exhibit alternance of heteroaromatic cores and electron withdrawing groups [19,20]. The absorption spectra of **BDTCOR** show that the effect of two thienoacetyl groups on **BDTA**, in terms of UV–Vis absorption amplitude and maxima values, is comparable, at least in the presence of alkoxy substituents [40], with that obtained by introduction of two bithienyl units [22]; hence, it represents a simple strategy to extend the electronic absorption to higher wavelengths. Furthermore, the electronic absorption spectrum of **BDT** shows the typical characteristics of rigid polycyclic aromatics, i.e. structured vibronic absorption bands and a very low value of the Stokes shift [39]. The maintenance of the vibronic structure, though blurred, and an increase of the Stokes shift are observable both in alkoxy derivatives of **BDT** [40] and in **BDTCOR**. The increase of the Stokes shift is attributable to a higher flexibility induced by the substituents: nevertheless, the maintenance of the vibronic structure suggests that the departure from planarity is scanty, in agreement with the reported calculated geometries, and mainly involves the alkoxy substituents.

A marked red-shift, due to the contribution of different functional groups, characterizes also the fluorescence spectra in apolar solvents, by passing from **BDT** to **BDTA** and then to **BDTCOR**: **BDT** is characterized by a structured band in methylcyclohexane with maxima at 336 and 353 nm [39] and **BDTCOR** by a maximum at 520 nm in cyclohexane, while **BDTA** shows an intermediate value of 385 nm [40].

A further important different property shown by **BDTCOR** regards

the value of the fluorescence quantum yield, ten-fold higher with respect to that of **BDT** (0.014 in ethanol [39]): such an increase, similar to that reported for **BDTA** [40], indicates a reduced competition of non-radiative paths of deactivation with respect to the fluorescence one. Therefore, the functionalization of **BDT** by alkoxy and thienoacetyl groups results also in an improvement of fluorescence properties, making **BDTCOR** a good fluorophore.

While the optical properties of (+)- and (±)-**BDTCOR** in solution are identical, the analysis of the absorption and fluorescence spectra of the films provides important indications on their different behavior in the solid state. Both the absorption and fluorescence spectra of the thin films deposited by physical vapor deposition from (±)-**BDTCOR** and (+)-**BDTCOR** show a bathochromic shift with respect to that obtained in solution (Fig. 3). Such observation indicates a strong π-π stacking intermolecular interaction in the film. The clear vibronic structure observable in absorption spectra of both films suggests the formation of highly ordered structures. Nevertheless, the films of (+)-**BDTCOR** and (±)-**BTDCOR** present different features in absorption and fluorescence spectra: a large red edge is observable in the absorption spectrum of the enantiopure form which is absent in that of the stereoisomer mixture. Since the excitation fluorescence spectrum does not show such an edge, this feature is attributable to the presence of non-fluorescent aggregates and/or to light scattering. Furthermore, the fluorescence spectra of (+)-**BDTCOR** is blue-shifted with respect to that of (±)-**BTDCOR.** Such differences lead us to suppose that different supramolecular organizations are adopted by the stereoisomer mixture and the pure enantiomer, as confirmed by morphological studies and ECD spectra (see later).

3.3. Circular dichroism measurements

ECD spectroscopy is an important tool for studying the perturbation induced by chiral substituents on π-conjugated systems and it is very sensitive to supramolecular chirality, which can characterize their aggregated states [41]. Therefore, the ECD spectrum of (+)-**BDTCOR** was recorded in solution, on casted film and on thin film obtained by vapor deposition technique.

The ECD spectrum of (+)-**BDTCOR** in THF (Fig. 4) does not present any detectable signal, indicating that the intrinsically achiral chromophore of **BDTCOR** is not perturbed by the chiral substituent in the isolated molecule.

On the contrary, a low Cotton effect is detected on films cast from different solvents (probably partially blurred by scattering phenomena), whereas the coating prepared by physical vapor deposition displays a structured bisignated Cotton effect (Fig. 4). This behavior is presumably due to exciton coupling, that points to the presence of a chiral architecture with negative helicity [41,42]. The two major peaks, one negative and one positive, are located at 493.5 nm (CDmdeg = −25.811, g = − 4.6 10^{-3}) and 367.5 nm (CDmdeg = 13.529, g = 3.4 10^{-2}),

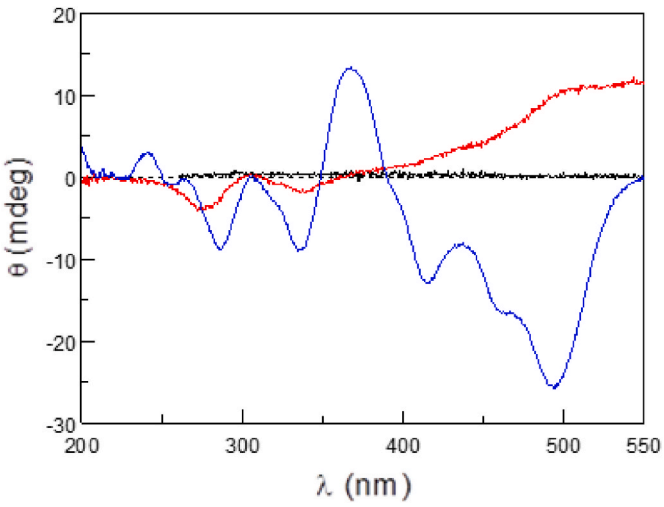

Fig. 4. ECD spectra of (+)-**BDTCOR** obtained on THF solution (black), film cast from o-dichlorobenzene (red) and film prepared by physical vapor deposition (blue).

respectively. They display g factors of the same order of those reported for a similar chiral BDT derivative [22]. A quite different behavior is observed for (±)-**BDTCOR** (Fig. S5), as expected. In fact, while (+)-**BDTCOR** exhibits a complex ECD spectrum, (±)-**BDTCOR** shows a flat ECD profile. These results strongly indicate that the (+)-**BDTCOR** coating obtained by physical vapor deposition is characterized by a chiral supramolecular architecture induced by the chiral substituent.

Summarizing, the UV–vis absorption spectrum of the films is red-shifted with respect to that of the monomer in solution. Though this could suggest, according to the exciton model proposed by Kasha [43] in the 1960s, the formation of J aggregates, such hypothesis is not supported by the red-shifted, broad and low-intensity fluorescence bands of the films, if compared with that in apolar solvents. As regards (+)-**BDTCOR**, the active ECD bands suggest the presence of a molecular assembly not simply ascribable to H or J aggregates, but to a twisted arrangement that gives rise to a chiral architecture with rotational symmetry, able to give both UV–vis and ECD active signals [42].

By comparing the ECD spectra of the (+)-**BDTCOR** films obtained by casting and physical vapor deposition method, it is possible to assess that a marked supramolecular order is present only in the second case.

Evidently, for these chiral carbonyl derivatives, the casting technique is not suitable to achieve an optimal supramolecular organization, contrary to what observed for similar chiral non-acetylated molecules [22]. On the other hand, as already reported by Deneme et al. vapor deposited films of molecules bearing the C═O group appear to be quite

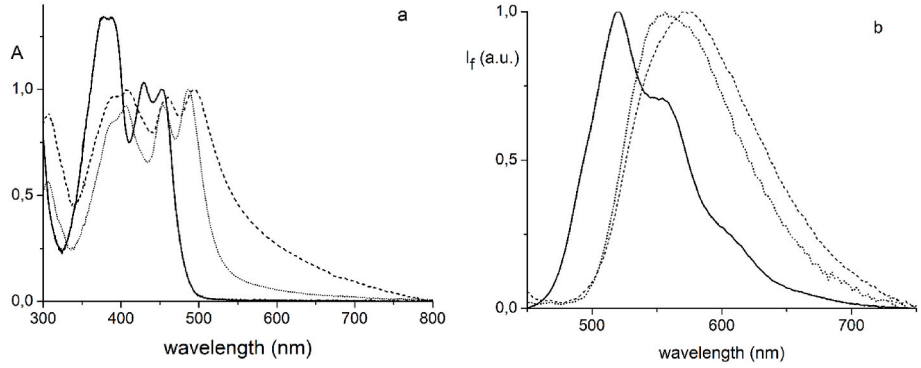

Fig. 3. a) Normalized absorption spectra of **BDTCOR** in cyclohexane (solid line) and of (+)-**BDTCOR** (dashed line) and (±)-**BDTCOR** (dotted line) as thin films deposited by thermal evaporation. b) Normalized fluorescence spectra of **BDTCOR** in cyclohexane (solid line) and of (+)-**BDTCOR** (dashed line) and (±)-**BDTCOR** (dotted line) as thin films (λex = 405 nm). Thickness of both films is 30 nm.

different from those obtained from analogous molecules where this functional group lacks [44]: the polar carbonyl group seems to induce strong intermolecular interactions which deeply influence the film morphology. In (+) BDTCOR both the chiral purity and the C═O polarity may play an important role on the molecular packing and then on the film quality.

3.4. Cyclic voltammetry

Figure S6 A and B report the voltammetric curves of (+)-**BDTCOR** and (±)-**BDTCOR**, respectively recorded in CH_3CN. As expected, the voltammetric curves of the two derivatives are very similar. In both cases, a p-doping process exhibiting two oxidation waves (I and II) attributable to the formation of cationic and dicationic species occurs, but the counterparts of the oxidation peaks are scarcely visible in the backward curve. In the cathodic region, a "quasi reversible" reduction process with the corresponding oxidation peak well visible in the backward curve is present. The peak potential values (E^p) found in the CVs are reported in Table 6. It is possible to use the CV curves to determine the onset potentials (E^{onset}) for the oxidation and reduction processes, and accordingly, to compute the electrochemical HOMO (E_{HOMO}) and LUMO (E_{LUMO}) energies according to the formulas [45]:

$$E_{HOMO} = -e[E^{onset}{}_{ox} + 4.4]$$

$$E_{LUMO} = -e[E^{onset}{}_{red} + 4.4]$$

Therefore, an evaluation of the band gap energy derived from electrochemical data is also possible (Eg_{electr}). The electrochemical parameters computed for (+)-**BDTCOR** and (±)-**BDTCOR** are reported in Table 6. As observable, the band gap values are well consistent with those computed by DFT and reported in Table S2.

3.5. Film morphology characterization

To explore the potential use of the here reported benzodithiophene derivatives as active materials in organic devices, as a preliminary study, we realized vacuum sublimed thin films on two different technological substrates extensively used for OTFT fabrication, i.e. SiO_2 and poly (methyl methacrylate) (PMMA).

In Fig. 5 a) and b), two representative images of (±)-**BDTCOR** film vacuum deposited on SiO_2 and on PMMA, respectively, are reported.

It is clearly visible that the chemical affinity of (±)-**BDTCOR** toward the PMMA surface plays a major role in determining the thin film molecular packing and morphology. In fact, in spite of the similar contact angle ($\approx 73^\circ$) of the SiO_2 and PMMA surfaces, they are characterized by very different surface chemistry. Dipolar –OH groups are indeed abundant on SiO_2 surface, while they are completely absent in PMMA. Considering the very low electric dipole associated to **BDTCOR**, a higher chemical affinity of molecules with the PMMA surface are expected at the local scale. This can account for the strong morphology differences evidenced by the AFM images for the thin films grown on the SiO_2 and the PMMA substrates, respectively. The poor chemical affinity with SiO_2 promotes a growth mechanism governed by the intermolecular interaction, which accumulate molecules in bigger scattered grains, preventing a uniform distribution of the molecules on the substrate. This situation is exactly depicted in Fig. 5a. On the other hand, the improved chemical affinity of the small molecules with the PMMA surface allows for (±)-**BDTCOR** the realization of quite uniform and connected thin

Table 6
Electrochemical parameters of **BDTCORs** in acetonitrile.

	E^{onset}_{ox} (V)	E^{p}_{oxI}(V)	E^{p}_{oxII}(V)	E^{onset}_{red} (V)	E^{p}_{red} (V)	Eg_{electr} (eV)
(±)-**BDTCOR**	+0.86	0.94	1.12	−1.37	−1.44	2.23
(+)-**BDTCOR**	+0.85	0.93	1.17	−1.37	−1.43	2.24

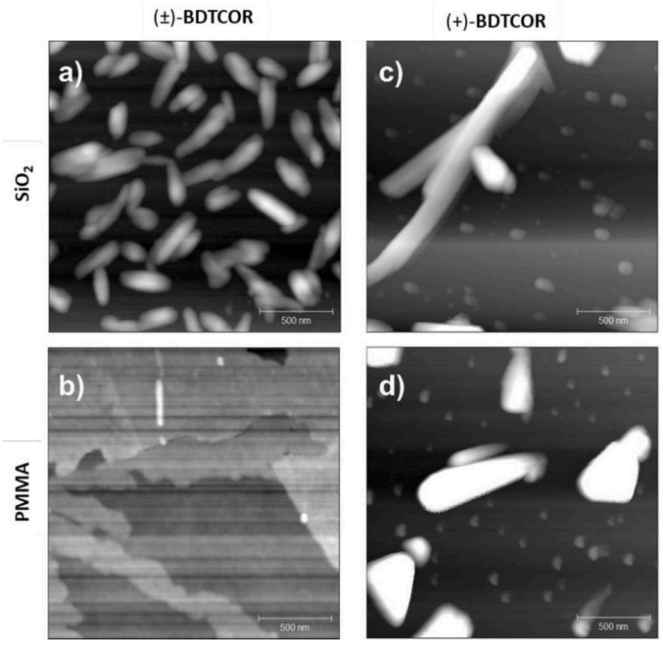

Fig. 5. AFM images of **BDTCORs**. a) 5 nm (±)-**BDTCOR** on SiO_2, b) 5 nm (±)-**BDTCOR** on PMMA, c) 30 nm (+)-**BDTCOR** on SiO_2, d) 30 nm (+)-**BDTCOR** on PMMA.

film, as highlighted by the AFM pictures of Fig. 5b. In more details, the (±)-**BDTCOR** film on PMMA shows a layer-by-layer growth mechanism characterized by the coalescence of large monolayer domains until the complete coverage of the substrate. The formation of the first monolayer is followed by the growth of the deposit *via* upper and upper layers, with an analogue mechanism. The minimum step measured between the different monolayers of Fig. 5b is about 1.5 nm and is compatible with a self-assembly structure in which the long axis of the molecules is perpendicular to the substrate surface. This organization, together with the presence of large domains, is in principle optimal for the realization of the active region in organic transistors *via* thermal vapor deposition technique [46].

The morphology of vacuum deposited (+)-**BDTCOR** thin films (1.8 nm thick, Fig. S7) is different from that observed for (±)-**BDTCOR**, especially in the case of PMMA. It is characterized by high isolated crystalline grains that extend out of plane following a tridimensional growth mechanism and no monolayers are detected. In particular, the surface wettability by (+)-**BDTCOR** molecules results so poor that the AFM images show only isolated small grains in the region between the crystalline domains. These grains result poorly visible also when the film thickness was enhanced to 30 nm (Fig. 5 c and d) and the AFM images reveal more or less the same morphology as the 1.8 nm thin films. This confirmed that the growth mechanism of (±)-**BDTCOR** and (+)-**BDTCOR** is different, especially on PMMA. The reason of these differences can be found in a stronger intermolecular interaction between the conjugated molecular cores of (+)-**BDTCOR**, possibly due to a higher order and compactness in the film packing, favored by the homochiral lateral chains, as inferred from ECD spectra. For (+)-**BDTCOR** the molecule-to-molecule interaction is more dominant than in (±)-**BDTCOR**, thus causing the formation of bigger and more isolated molecular domains on SiO_2, as the comparison of Fig. 5a and c shows. Again, when deposited on a substrate having a better chemical affinity, as in the case for PMMA, the growth mechanism of (+)-**BDTCOR** remains strongly tridimensional (Fig. 5d), while (±)-**BDTCOR** shows a drastic growth change towards a layer-by-layer mechanism (Fig. 5b).

This preliminary study shows that the (±)-**BDTCOR** molecular thin film organization can be controlled using an *ad-hoc* optimization of the

substrate surface chemistry. In particular, an ordered film with a vertical molecular orientation favorable for the in-plane charge transport can be achieved using, for example, a PMMA layer as the substrate (Fig. 5b). (+)-**BDTCOR**, instead, independently of the substrate, tends to aggregate in big crystalline structures. In light of this, both (+)- and (±)-**BDTCOR** can be considered interesting candidates for the realization of the organic transistor active region. The transistor transporting film can be realized using a thermal vapor deposition process for (±)-**BDTCOR**, while a single crystal approach is necessarily required for (+)-**BDTCOR**. This latter configuration has been successfully explored for other BDT-core based compounds [47].

4. Conclusions

In this paper, a BDT-based small molecule in stereoisomer mixture, (±)-**BDTCOR**, and enantiopure form, (+)-**BDTCOR**, was synthesized and characterized. The spectroscopic measurements show that **BDTCOR** is wide absorbing, revealing that a simple ketonic group has the ability to significantly shift the absorption spectrum to longer wavelengths, thanks to the extended conjugation pathway. The optical properties of the films indicate a further red-shift of the low-energy absorption band, if compared with that in solution. Furthermore, a strong intermolecular π-π stacking takes place, which is a favorable property for application in optoelectronic devices. In the case of (+)-**BDTCOR**, ECD spectrum shows that the aggregate phase is characterized by a left-handed helicity arrangement of the π-conjugated core. Spectroscopic and morphological analysis show that (±)-**BDTCOR** and (+)-**BDTCOR** as vapor-deposited films organize themselves in different structures, less and more ordered for (±)-**BDTCOR** and (+)-**BDTCOR**, respectively. This is probably the consequence of the different arrangement of π-stack aggregates induced by the hetero- and homochiral substituents. (+)-**BDTCOR** is completely dominated by the intermolecular interaction and it grows forming isolated crystallites, independently of the substrate used. In spite of the evidence of a clear intermolecular interaction also for (±)-**BDTCOR**, the growth morphology can be controlled exploiting the interaction with the substrate in this case, inducing a layer-by-layer growth mechanism that ensure the formation of planar and well-connected thin films at the nanometric scale. These results, together with the strong π-π molecular interaction, make (±)-**BDTCOR** potentially suitable for thin film based organic electronic applications. The ECD spectra observed for vapor-deposited (+)-**BDTCOR** film clearly shows the presence of chiral supramolecular structures which are absent in solution and in casted films, showing the great impact of the deposition technique on the supramolecular organization of the material. This opens the way for further deeper studies on the use of these molecules as active materials in optoelectronic devices where the interaction with circularly polarized light is required.

Declaration of competing interest

The authors declare that they have no known competing financial interests or personal relationships that could have appeared to influence the work reported in this paper.

Data availability

Data will be made available on request.

Appendix A. Supplementary data

Supplementary data to this article can be found online at https://doi.org/10.1016/j.optmat.2023.113619.

References

[1] S.D. Collins, N.A. Ran, M.C. Heiber, T.Q. Nguyen, Adv. Energy Mater. 7 (2017), https://doi.org/10.1002/aenm.201602242.
[2] S.J. Cho, M.J. Kim, Z. Wu, J.H. Son, S.Y. Jeong, S. Lee, J.H. Cho, H.Y. Woo, ACS Appl. Mater. Interfaces 12 (2020) 41842–41851.
[3] B.J. Rancatore, B.S. Kim, C.E. Mauldin, J.M.J. Fréchet, T. Xu, Macromolecules 49 (2016) 833–843.
[4] H. Bin, J. Yao, Y. Yang, I. Angunawela, C. Sun, L. Gao, L. Ye, B. Qiu, L. Xue, C. Zhu, C. Yang, Z.G. Zhang, H. Ade, Y. Li, Adv. Mater. 30 (2018) 1–8.
[5] H. Yao, L. Ye, H. Zhang, S. Li, S. Zhang, J. Hou, Chem. Rev. 116 (2016) 7397–7457.
[6] X. Hao, M. Liang, X. Cheng, X. Pian, Z. Sun, S. Xue, Org. Lett. 13 (2011) 5424–5427.
[7] C. Wang, H. Dong, W. Hu, Y. Liu, D. Zhu, Chem. Rev. 112 (2012) 2208–2267.
[8] Y. Liang, Z. Xu, J. Xia, S.T. Tsai, Y. Wu, G. Li, C. Ray, L. Yu, Adv. Mater. 22 (2010) 135–138.
[9] S. Park, B.T. Lim, B. Kim, H.J. Son, D.S. Chung, Sci. Rep. 4 (2014), https://doi.org/10.1038/srep05482.
[10] N. Sylvianti, Y.H. Kim, M.A. Marsya, D.G. Kim, B.H. Ahn, S.S. Hong, J.H. Kim, Mol. Cryst. Liq. Cryst. 660 (2018) 66–71.
[11] W. Wang, G. Wang, J. Yang, J. Zhang, L. Chen, C. Weng, Z.G. Zhang, Y. Li, P. Shen, Chem. Phys. Lett. 672 (2017) 63–69.
[12] S. Nishinaga, H. Mori, Y. Nishihara, J. Org. Chem. 83 (2018) 5506–5515.
[13] G. Zhao, J. Liu, Q. Meng, D. Ji, X. Zhang, Y. Zou, Y. Zhen, H. Dong, W. Hu, G. Zhao, J. Liu, Q. Meng, D. Ji, X. Zhang, Y. Zou, Y. Zhen, H. Dong, W. Hu, 2015, DOI 10.1002/aelm.201500071.
[14] J. Yagui, F.A. Angel, Opt. Mater. 109 (2020), 110354.
[15] Y. Duan, X. Xu, L. Yu, Y. Li, R. Li, Q. Peng, Dyes Pigments (2021) 191, https://doi.org/10.1016/j.dyepig.2021.109387.
[16] H. Tang, C. Yan, J. Huang, Z. Kan, Z. Xiao, K. Sun, G. Li, S. Lu, Matter 3 (2020) 1403–1432.
[17] A. Venkateswararao, K.-T. Wong, Bull. Chem. Soc. Jpn. 94 (2021) 812–838.
[18] N. I. Wakayama, M. Wakayama, *Jpn. J. Appl. Phys.* n.d., DOI 10.1143/JJAP.46.L727.
[19] T. Bilkay, K. Schulze, T. Egorov-Brening, K. Fink, S. Janietz, Org. Electron. 14 (2013) 344–353.
[20] C. Uhrich, R. Schueppel, A. Petrich, M. Pfeiffer, K. Leo, E. Brier, P. Kilickiran, P. Baeuerle, Adv. Funct. Mater. 17 (2007) 2991–2999.
[21] L. Yuan, K. Lu, B. Xia, J. Zhang, Z. Wang, Z. Wang, D. Deng, J. Fang, L. Zhu, Z. Wei, Adv. Mater. 28 (2016) 5980–5985.
[22] G. Albano, M. Lissia, G. Pescitelli, L.A. Aronica, L. Di Bari, Mater. Chem. Front. 1 (2017) 2047–2056.
[23] G. Albano, F. Salerno, L. Portus, W. Porzio, L.A. Aronica, L. Di Bari, ChemNanoMat 4 (2018) 1059–1070.
[24] L. Wan, J. Wade, F. Salerno, O. Arteaga, B. Laidlaw, X. Wang, T. Penfold, M. J. Fuchter, A.J. Campbell, ACS Nano 13 (2019) 8099–8105.
[25] Y. Yang, R.C. Da Costa, D.M. Smilgies, A.J. Campbell, M.J. Fuchter, Adv. Mater. 25 (2013) 2624–2628.
[26] D.W. Zhang, M. Li, C.F. Chen, Chem. Soc. Rev. 49 (2020) 1331–1343.
[27] J.R. Brandt, X. Wang, Y. Yang, A.J. Campbell, M.J. Fuchter, J. Am. Chem. Soc. 138 (2016) 9743–9746.
[28] R. Singh, K.N. Narayanan Unni, A. Solanki, Deepak, *Opt Mater (Amst)* 34 (2012) 716–723.
[29] E. Togan, Y. Chu, A.S. Trifonov, L. Jiang, J. Maze, L. Childress, M.V.G. Dutt, A. S. Sørensen, P.R. Hemmer, A.S. Zibrov, M.D. Lukin, Nature 466 (2010) 730–734.
[30] W. Ma, L. Xu, L. Wang, C. Xu, H. Kuang, Adv. Funct. Mater. 29 (2019), https://doi.org/10.1002/adfm.201805512.
[31] D. Magde, R. Wong, P.G. Seybold, Photochem. Photobiol. 75 (2002) 327.
[32] F. Neese, J. Wiley, WIREs Comput Mol Sci 2 (2012) 73–78.
[33] F. Neese, WIREs Comput Mol Sci 8 (2018) 1327.
[34] J. Tomasi, B. Mennucci, R. Cammi, 2005, DOI 10.1021/cr9904009.
[35] Orca 5.02 Manual @canbe found under, https://orcaforum.kofo.mpg.de/.
[36] P. Morvillo, F. Parenti, R. Diana, C. Fontanesi, A. Mucci, F. Tassinari, L. Schenetti, Sol. Energy Mater. Sol. Cell. 104 (2012) 45–52.
[37] M. Caselli, D. Vanossi, M. Buffagni, M. Imperato, L. Pigani, A. Mucci, F. Parenti, Chempluschem 84 (2019) 1314–1323.
[38] F. Terenziani, A. Painelli, C. Katan, M. Charlot, M. Blanchard-Desce, J. Am. Chem. Soc. 128 (2006) 15742–15755.
[39] B. Wex, B.R. Kaafarani, E.O. Danilov, D.C. Neckers, J. Phys. Chem. A 110 (2006) 13754–13758.
[40] T.M. Pappenfus, D.T. Seidenkranz, M.D. Lovander, T.L. Beck, B.J. Karels, K. Ogawa, D.E. Janzen, J. Org. Chem. 79 (2014) 9408–9412.
[41] N. Harada, K. Nakanishi, Circular Dichroic Spectroscopy: Exciton Coupling In Organic Stereochemistry, 1983.
[42] G. Albano, G. Pescitelli, L. Di Bari, Chem. Rev. 120 (2020) 10145–10243.
[43] R. H. R, M. A, E.-B.M. Kasha, Pure Appl. Chem. 11 (1965) 371–392.
[44] I. Deneme, G. Liman, A. Can, G. Demirel, H. Usta, Nat. Commun. 12 (2021) 1–11.
[45] C.M. Cardona, W. Li, A.E. Kaifer, D. Stockdale, G.C. Bazan, Adv. Mater. 23 (2011) 2367–2371.
[46] R. Capelli, M.V. Nardi, T. Toccoli, R. Verucchi, F. Dinelli, C. Gelsomini, K. Koshmak, A. Giglia, S. Nannarone, L. Pasquali, Appl. Phys. Lett. 112 (2018), https://doi.org/10.1063/1.5008941.
[47] H. Takenaka, T. Ogaki, C. Wang, K. Kawabata, K. Takimiya, 2019, DOI 10.1021/acs.chemmater.9b01187.